Inorganic Chemistry

Article

pubs.acs.org/IC

A Ferrimagnetic Zintl Phase Pr_4MnSb_9: Synthesis, Structure, and Physical Properties

Xiong Chen,[†,‡] Jin-Ni Shen,[†,‡] Li-Ming Wu,[†] and Ling Chen*[,†]

[†]Key Laboratory of Optoelectronic Materials Chemistry and Physics, Fujian Institute of Research on the Structure of Matter, Chinese Academy of Sciences, Fuzhou, Fujian 350002, People's Republic of China

[‡]University of Chinese Academy of Sciences, Beijing 100039, People's Republic of China

Supporting Information

ABSTRACT: A new valence precise Zintl phase, Pr_4MnSb_9, has been successfully synthesized by solid-state reaction at high temperature. The single-crystal X-ray diffraction data reveal its monoclinic symmetry in the space group $C2/m$ (No. 12) with a = 24.12(2) Å, b = 4.203(3) Å, c = 15.67(2) Å, β = 98.05(1)°, and Z = 4. The structure is characterized by the covalent three-dimensional network constructed by two types of five-atom-wide Sb_5^{7-} ribbons that are joined by 6-fold coordinated Mn^{3+} cations, through which the narrower three-atom-wide Sb_3^{5-} ribbons are attached as a tag, and interstitial Pr^{3+} cations and single Sb^{3-} anions locate within the tunnels. Its magnetic susceptibility and isothermal hysteresis suggest ferrimagnetic behavior. The electrical conductivity and Seebeck coefficient of the cold-pressed pellet suggest a semimetal feature that agrees with the spin-polarized calculation results using the tight-binding linear muffin-tin orbital (TB-LMTO) method.

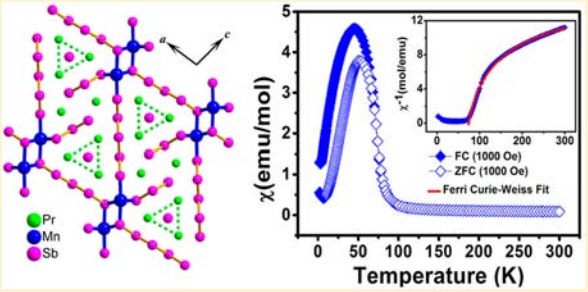

INTRODUCTION

Ternary rare-earth antimonides exhibit interesting physical properties[1,2] and diverse structural chemistry of the anionic Sb substructures in the forms of ring, cluster, chain, ribbon, and network, with a wide range of Sb−Sb bonding interactions.[3−5] Among them, RE/Mn/Sb compounds are of particular interest because their components provide abundant f and d electrons that may give rise to interesting magnetic interactions, some examples are RE_6MnSb_2 (RE = Ho, Er, Lu),[6,7] $RE_{14}MnSb_{11}$ (RE = Eu, Yb),[8,9] $Eu_{10}Mn_6Sb_{13}$,[10,11] $REMn_2Sb_2$ (RE = Eu, Yb),[12,13] $REMn_{1-x}Sb_2$ (RE = La−Nd, Sm),[14−16] RE_6MnSb_{15} (RE = La, Ce),[17,18] and $Yb_9Mn_{4+x}Sb_9$,[19] and so on. In Er_6MnSb_2, the (1 0 0) layers of Er^{3+} atoms show a ferromagnetic ordering below 110 K, and Mn sites show no local moment.[7] $Eu_{10}Mn_6Sb_{13}$ is paramagnetic with a ferromagnetic component present below 60 K, and complete ordering of Eu sublattices at 4.2 K.[10] $YbMn_2Sb_2$ exhibits an antiferromagnetic coupling of Mn^{2+} sites with no magnetic moment coming from Yb^{2+} sites below 120 K.[13] $PrMnSb_2$ presents an antiferromagnetic ordering of the Mn^{3+} moments at ∼175 K, and an antiferromagnetic ordering of Pr^{3+} moments at ∼35 K.[15,16]

Here, we report a new Zintl phase compound, Pr_4MnSb_9. Syntheses, single crystal structure characterizations, magnetic property analyses as well as the theoretic discussions are presented.

EXPERIMENTAL SECTION

Synthesis. Handling of all materials was carried out in an Ar-filled glovebox with controlled oxygen and moisture levels. Rare-earth metals were purchased from Huhhot Jinrui Rare Earth Co. Ltd. Mn (99.99%) and Sb (99.99%) were purchased from Alfa Aesar China (Tianjin) Co. Ltd. Compound Pr_4MnSb_9 was first discovered in the reaction targeting at a proposed "$Pr_6Mn_{1.2}Sb_{14.6}$", an analogue of $Pr_6Zn_{1.2}Sb_{14.6}$.[20] After establishing its structure, the pure phased Pr_4MnSb_9 compound was synthesized by the stoichiometric reactions of Pr, Mn, and Sb elements in a carbon coated silica tube, which was flame-sealed under a vacuum of 10^{-3} Pa. The reaction assembly was then heated in a temperature controlled tube furnace to 1373 at 25 K/h, followed by dwelling for 20 h, and then cooling at 4 K/h to 373 K before shutting down the furnace. The powder X-ray diffraction pattern of the product matched well with the one simulated from the single-crystal data. (Figure 1) Similar attempts with other rare earth metals, La, Ce, Nd, Sm, and Gd, for the proposed isostructural RE_4MnSb_9 only yielded the known RE_6MnSb_{15}.[17,18]

Single-Crystal Structure Determination. Single crystal diffraction data were collected on a Rigaku Mercury CCD diffractometer equipped with a graphite-monochromatic Mo Kα radiation (λ = 0.71073 Å) at room temperature. Absorption corrections based on the multiscan method[21] were applied. The structure was solved by the direct method and refined on F^2 by full-matrix least-squares methods using the SHELX-97 software package.[22] All of the atoms were refined with the anisotropic displacement parameters and a secondary extinction correction. Atomic positions were standardized with the STRUCTURE TIDY program.[23] Table 1 summarized crystallographic data and structural refinements.

Powder X-ray Diffraction. The XRD data were collected at room temperature on a Rigaku DMAX 2500 diffractometer by using monochromatized Cu Kα radiation (λ = 1.5418 Å) in the range of 2θ

Received: January 28, 2013
Published: June 7, 2013

   dx.doi.org/10.1021/ic400209x | Inorg. Chem. 2013, 52, 7441−7447

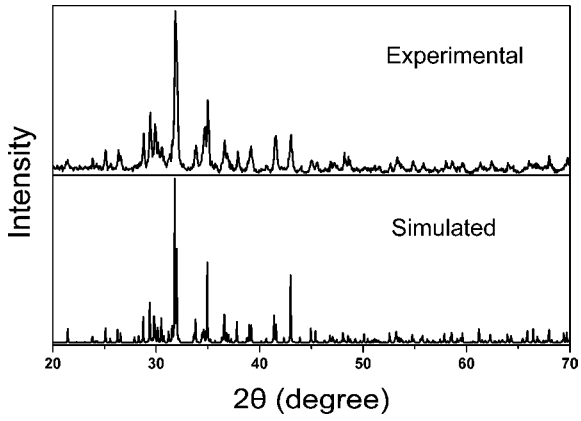

Figure 1. Experimental and simulated X-ray powder diffraction patterns of Pr_4MnSb_9.

Table 1. Crystal Data and Structural Refinements for Pr_4MnSb_9

formula	Pr_4MnSb_9
formula weight	1714.33
space group	$C2/m$
a (Å)	24.12(2)
b (Å)	4.203(3)
c (Å)	15.67(2)
β (deg.)	98.05(1)
V (Å^3)	1573(2)
Z	4
temperature (K)	293(2)
ρ_{cal} (g/cm^3)	7.241
μ (Mo Kα) (mm^{-1})	28.031
R1, wR2 $[I > 2\sigma(I)]^a$	0.0355, 0.0931
R1, wR2 (all data)	0.0387, 0.0975
goodness of fit on F^2	1.098
largest diff. peak and hole (e·Å^{-3})	2.950, −1.695

$^aR_1 = \sum||F_o| - |F_c||/\sum|F_o|$, $wR_2 = [\sum w(F_o^2 - F_c^2)^2/\sum w(F_o^2)^2]^{1/2}$.

= 20−70° with a scan step width of 0.05°. The measured XRD pattern was in good agreement with the simulated one (Figure 1).

Elemental Analyses. The Pr, Mn, and Sb element analyses were carried out with the aid of a field emission scanning electron microscope (FESEM, JSM6700F) equipped with an energy dispersive X-ray spectrometer (EDX, Oxford INCA) on the same Pr_4MnSb_9 crystal used for single crystal diffraction analyses. The EDX results indicated the presence of Pr, Mn, and Sb with average atomic percentages (atom %) of Pr, 28.9(6); Mn, 6.9(1); and Sb, 64.1(3), which were in good agreement with the single crystal refinement results: (atom %): Pr, 28.6; Mn, 7.1; and Sb, 64.3. (Supporting Information, Figure S1)

Magnetic Measurements. Magnetic susceptibilities of Pr_4MnSb_9 were measured on a Quantum Design PPMS-9T magnetometer between 2 and 300 K. The 20−40 mg hand picked crystals were ground to fine powders to minimize the anisotropic effect and loaded into a gelatin capsule. The magnetization temperature dependence was measured under a constant magnetic field of 1000 Oe. The field dependent magnetization were measured at 2 and 60 K via sweeping through fields from 0 to 8, 8 to −8 and −8 to 8 T, respectively. Corrections for contributions from the container and the ion-core diamagnetism were applied.

Differential Thermal Analysis and Thermogravimetric Analyses (DTA/TGA). Thermal stability was tested using Netzsch STA 449 F3 on a polycrystalline sample of Pr_4MnSb_9 (30 mg) under a high-purity N_2 flow with pressure of 0.05−0.1 MPa and flow velocity of 20 mL/min from 300 to 973 K with a heating rate of 30 K/min.

Electrical Conductivity and Seebeck Coefficient Measurements. Electrical conductivity and Seebeck coefficient were measured on a cold-pressed 2.1 × 2.0 × 9.1 mm^3 bar shaped polycrystalline pellet with ∼73% theoretical density on an ULVAC-RIKO ZEM-3 instrument by the four-probe method under flowing Ar atmosphere. The data were measured three times in the temperature range to ensure the reliability of the data.

Electronic Structure Calculations. Calculations based on the tight-binding linear muffin-tin orbital (TB-LMTO) method were carried out within the local density and atomic sphere approximations using the TB-LMTO-ASA 4.7 program.[24] The basis sets include 6*s*, 6p, 5d, 4f for Pr, 4s, 4p, 3d for Mn, 5s, 5p, 5d for Sb, and s, p, and d for "empty" (ES), respectively. The one-electron self-consistent potentials had been obtained by performing iterations on a grid of 192 points in the entire Brillouin zone. The tetrahedral method had been used to calculate the electron density of states. The accuracy in the energy convergence was 10^{-5} Ry.

RESULTS AND DISCUSSION

Crystal Structure. Pr_4MnSb_9 with its own structure type crystallizes in the space group $C2/m$ with a = 24.12(2) Å, b = 4.203(3) Å, c = 15.67(2) Å, β = 98.05(1)°, and Z = 4 (Table 1). The major structure features a new three-dimensional (3D) network constructed by three types of Sb ribbons (denoted as A, B, and C, hereafter) that are noded by Mn atoms (Figure 2). The isolated Pr^{3+} cations and single $Sb1^{3-}$ anions locate within the tunnels (Figure 2).

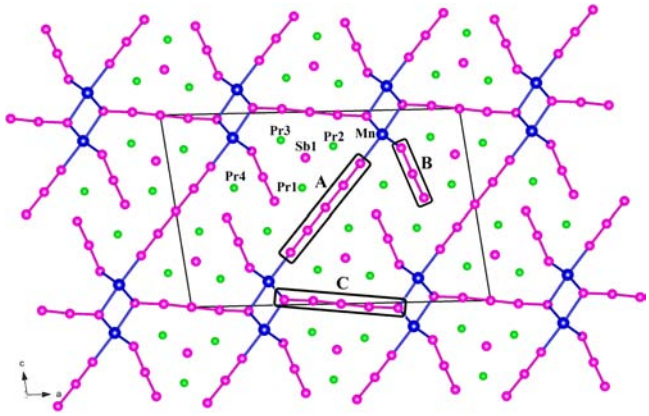

Figure 2. Pr_4MnSb_9 structure viewed down the *b*-axis with unit cell outlined. Green, Pr^{3+}; dark blue, Mn^{3+}; purple, Sb atoms of which $Sb1^{3-}$ is labeled. A, C: five-atom-wide $(Sb_5)^{7-}$ polyanion ribbons, B: three-atom-wide $(Sb_3)^{5-}$ polyanion ribbon.

As detailed in Figure 3, ribbon A is a five-atom-wide Sb ribbons with a width of 9.08 Å constructed by the Sb2, Sb3, and Sb4 atoms. Such a ribbon is a nonclassical polyanion constructed by electron rich multicenter bonding (i.e., hypervalent bonding) according to Hoffmann.[3a] Accordingly, Sb3 and Sb4 (4-fold coordinated by neighboring Sb atoms) are therefore assigned as Sb^- anions, and the 2-fold coordinated Sb2 is assigned as Sb^{2-} anion. Thus, ribbon A can be denoted as $[(Sb2)^{2-}]_2[(Sb3)^-]_2(Sb4)^- \equiv (Sb_5)^{7-}$. Alternatively, the electron counting can be understood as following: the repeat unit Sb2−Sb3−Sb4−Sb3−Sb2 forms two perpendicular six-electron five-center bonds, therefore 8 electrons should be excluded from the antibonding orbitals. Consequently, the Sb_5 group should carry 15−8 = 7 electrons, that is, $(Sb)_5^{7-}$. Similarly, the three-atom-wide B ribbon with a width of 4.43 Å consists 4-fold coordinated Sb6 and 2-fold coordinated Sb5, Sb7 that can be denoted as $B \equiv (Sb_3)^{5-}$. Ribbon C is a five-

dx.doi.org/10.1021/ic400209x | *Inorg. Chem.* 2013, 52, 7441−7447

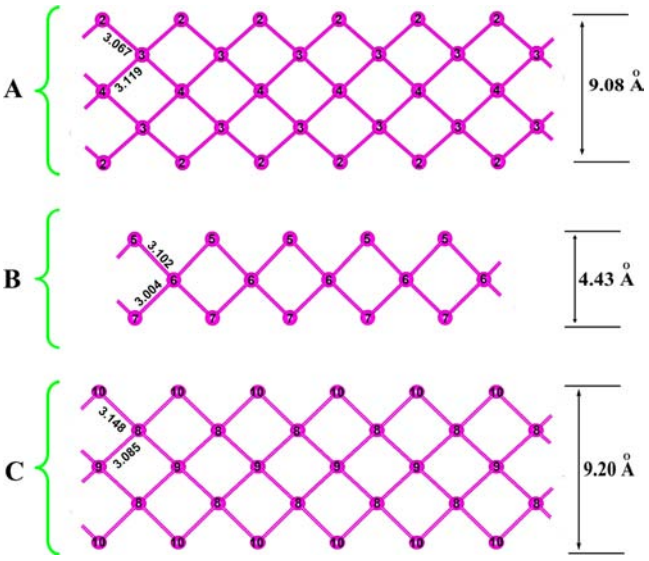

Figure 3. Fragments of polyanion Sb ribbons extending along the *b* axis in Pr_4MnSb_9. The local coordination of each Sb is also presented. The formula of each ribbon is as follows, A: $[(Sb2)^{2-}]_2[(Sb3)^-]_2(Sb4)^- \equiv (Sb_5)^{7-}$; B: $(Sb5)^{2-}(Sb6)^-(Sb7)^{2-} \equiv (Sb_3)^{5-}$; and C: $[(Sb8)^-]_2(Sb9)^-[(Sb10)^{2-}]_2 \equiv (Sb_5)^{7-}$. The widths of these ribbons are shown at the right side. The Sb−Sb distance is within 3.2 Å.

atom-wide ribbon made by Sb8−10, with a slightly wider width of 9.20 Å that is written as $C \equiv (Sb_5)^{7-}$. Therefore, compound Pr_4MnSb_9 can be described as $(Pr^{3+})_8(Mn^{3+})_2(Sb1^{3-})_2A^{7-}C^{7-}(B^{5-})_2$ that equals to a valence precise $(Pr^{3+})_8(Mn^{3+})_2(Sb^{3-})_2[(Sb_5)^{7-}]_2[(Sb_3)^{5-}]_2$. Such a Zintl formalism with formal charge reflects the covalent Sb−Sb bonding interaction within the 3D anionic framework. The Sb−Sb bond lengths (3.004 to 3.148 Å) are comparable with those of La_6MnSb_{15} (2.882 to 3.504 Å) [17] and $Pr_6Zn_{1.2}Sb_{14.6}$ (2.797 to 3.621 Å) [20]. On the other hand, the formal charge of each Sb atoms can be also calculated by the bond-valence sums introduced by Jeitschko,[3b,c] as listed in Supporting Information, Table S1; the results agree with those based on the hypervalent bonding concept.[3a] (Table 2)

The Mn atoms are 6-fold coordinated by one Sb2, two Sb7, and three Sb10 atoms in a distorted octahedron environment, and serve as nodes to join ribbons A and C into a 3D network. The narrow B ribbons are attached to the framework via Mn atoms as hanging tags. (Figure 2, Supporting Information, Figure S2) The Mn−Sb bond lengths range from 2.818(2) to 2.913(4) Å (Table 3), which are comparable with 2.826(1) Å in MnSb.[25] Besides, the XPS measurements indicate that the formal valence state of Mn in title Pr_4MnSb_9 can be considered the same as that in MnSb,[25] that is +3. (Supporting Information, Figure S5)

Table 3. Selected Bond Lengths (Å) in Pr_4MnSb_9

bond	dist.	bond	dist.
Pr1−Sb1 × 2	3.217(2)	Pr4−Sb2 × 2	3.305 (2)
Pr1−Sb3	3.320(3)	Pr4−Sb3	3.244(3)
Pr1−Sb3	3.434(3)	Pr4−Sb5 × 2	3.223(2)
Pr1−Sb4 × 2	3.243(2)	Pr4−Sb5	3.424(3)
Pr1−Sb5 × 2	3.258(2)	Pr4−Sb6 × 2	3.260(2)
Pr1−Sb6	3.279(3)	Pr4−Sb7	3.297(3)
Pr2−Sb1 × 2	3.214(2)	Mn−Sb2	2.944(4)
Pr2−Sb2 × 2	3.334(2)	Mn−Sb7 × 2	2.818(2)
Pr2−Sb3	3.278(3)	Mn−Sb10 × 2	2.862(3)
Pr2−Sb8 × 2	3.294(2)	Mn−Sb10	2.913(4)
Pr2−Sb9	3.346(2)	Sb2−Sb3 × 2	3.067(2)
Pr2−Sb10	3.620(3)	Sb3−Sb4 × 2	3.119(2)
Pr3−Sb1 × 2	3.222(2)	Sb3−Sb5	4.118(3)
Pr3−Sb6	3.316(3)	Sb5−Sb6 × 2	3.004(2)
Pr3−Sb7 × 2	3.274(2)	Sb6−Sb7 × 2	3.102(2)
Pr3−Sb8 × 2	3.285(2)	Sb8−Sb9 × 3	3.085(2)
Pr3−Sb9	3.262(2)	Sb8−Sb10 × 2	3.148(2)
Pr3−Sb10	3.452(3)		

All Pr atoms serve as interstitial cations that are coordinated in distorted tricapped trigonal prisms defined by six Sb atoms and three capping Sb atoms (Supporting Information, Figure S2). The Pr−Sb lengths vary from 3.214(2) to 3.620(3) Å, which are comparable with those in $Pr_6Zn_{1.2}Sb_{14.6}$ (3.240(2) to 3.366(6) Å).[20] Differently, Sb1 at a 4*i* site is considered as a single Sb^{3-} anion that is surrounded by six Pr^{3+} cations with distance around 3.2 Å (Supporting Information, Figure S2).

Table 2. Atomic Coordinates and Equivalent Isotropic Displacement Parameters of Pr_4MnSb_9

atom	valence state	Wyckoff site	*x*	*y*	*z*	U_{eq}(Å)[a]
Pr1	+3	4*i*	0.06649(4)	0	0.39360(5)	0.0052(2)
Pr2	+3	4*i*	0.05958(4)	0	0.81954(5)	0.0068(3)
Pr3	+3	4*i*	0.11193(4)	0	0.14348(5)	0.0061(2)
Pr4	+3	4*i*	0.20616(4)	0	0.61250(7)	0.0063(2)
Mn	+3	4*i*	0.2706(2)	0	0.1253 (2)	0.0171(7)
Sb1	−3	4*i*	0.53948(5)	0	0.23787(7)	0.0062(3)
Sb2	−2	4*i*	0.36004(5)	0	0.27397(7)	0.0085(3)
Sb3	−1	4*i*	0.07176(5)	0	0.61377(7)	0.0088(3)
Sb4	−1	2*d*	0	0.5	0.5	0.0061(3)
Sb5	−2	4*i*	0.33356(5)	0	0.53977(7)	0.0071(3)
Sb6	−1	4*i*	0.19153(4)	0	0.33405(7)	0.0077(3)
Sb7	−2	4*i*	0.71490(5)	0	0.19786(7)	0.0088(3)
Sb8	−1	4*i*	0.40891(5)	0	0.01902(7)	0.0088(3)
Sb9	−1	2*a*	0	0	0	0.0082(4)
Sb10	−2	4*i*	0.81276(6)	0	0.02838(9)	0.0210(3)

[a] U(eq) is defined as one-third of the trace of the orthogonalized U_{ij} tensor.

dx.doi.org/10.1021/ic400209x | Inorg. Chem. 2013, 52, 7441−7447

Note that the stoichiometry of Pr_4MnSb_9 is very close to a known $Pr_6Zn_{1.2}Sb_{14.6} \equiv Pr_4Zn_{0.8}Sb_9$.[20] Both compounds have three-atom-wide ribbons of $(Sb_3)^{5-}$ and single Sb^{3-} anions coordinated in trigonal prisms. Differently, in $Pr_6Zn_{1.2}Sb_{14.6}$,[20] the four-atom-wide Sb_4 ribbons are linked into a 3D network by Sb−Sb pairs through Sb−Sb bonding interactions, yet, in the title compound Pr_4MnSb_9, the five-atom-wide Sb_5 ribbons are linked into a 3D network by two Mn nodes with no Mn−Mn bonding interaction. Second, the "roles" of transition metals are distinct. In $Pr_6Zn_{1.2}Sb_{14.6}$, Zn atoms are square pyramidal or tetrahedral coordinated and serve as interstitials; yet, in Pr_4MnSb_9, Mn atoms are 6-fold coordinated and act as nodes. Besides, from the crystallographic point of view, partial occupancies happen in $Pr_6Zn_{1.2}Sb_{14.6}$ at Zn sites at 4*j* and 4*h*, Sb sites at 4*g* and 2*a*, but not in Pr_4MnSb_9 (Figure 4).

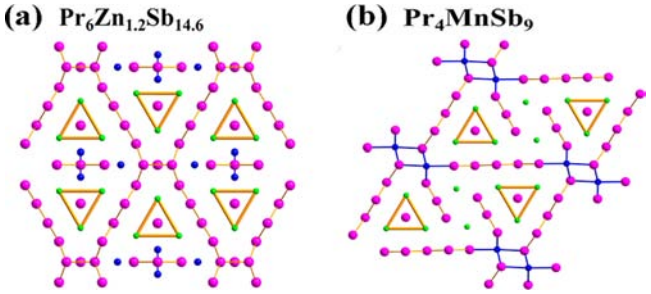

Figure 4. Structure projections down the shortest axis of (a) $Pr_6Zn_{1.2}Sb_{14.6}$,[20] and (b) Pr_4MnSb_9. Green, Pr; dark blue, Zn or Mn; purple, Sb. Trigonal prism M_6Sb around the single Sb atom (i.e., Sb^{3-}) is outlined by golden lines.

Magnetic Properties. Figure 5 shows the susceptibility temperature dependence of polycrystalline Pr_4MnSb_9 at H = 1000 Oe with an inset of the inverse susceptibility, which obeys the Curie−Weiss law $\chi = C/(T - \theta)$ in the temperature range of 200−300 K with Curie constant (C) = 49.65 emu K/mol and Weiss temperature (θ) = −259.67 K. The negative Weiss temperature suggests a significant antiferromagnetic correlation between the magnetic ions. The magnetization temperature dependence shows a transition temperature at ∼74 K, near which a pronounced curvature of the inverse susceptibility is observed. A similar behavior has been attributed to a ferrimagnetic ordering in $MO{\cdot}Fe_3O_4$ (M = Mg, Fe, Co, Ni, Cu, Zn, Cd),[26] and $Ca_{21}Mn_4Sb_{18}$.[27] The high temperature data $(T > T_C)$ can be fit to a ferrimagnetic Curie model with T_C = 74.27(8) K under the approximation that two magnetic sites are separated, that is, $\chi = [(C_A + C_B)T - 2\mu C_A C_B]/(T^2 - T_C^2) + \chi_0$.[26] The fit line is shown as a red solid line in the inset in Figure 5, and the corresponding parameters are listed in Table 4. The goodness of fit as shown in Figure 5 proves that the proposed ferrimagnetic model is reasonable. The observed effective moment μ_{eff} = 8.13(5) μ_B is comparable with but deviates from the calculated μ_{eff} = 8.67 μ_B. Detailed magnetic property studies, including theanisotropic magnetic susceptibility contribution from the itinerant 3d electrons, are worthy of doing.

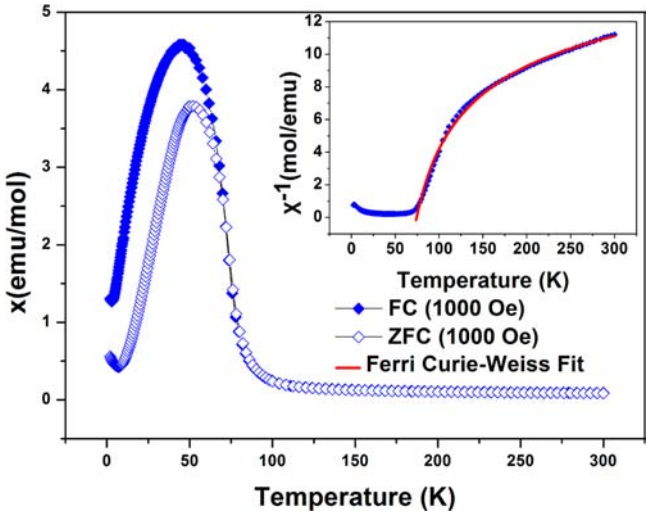

Figure 5. Temperature dependence of the magnetic susceptibility of polycrystalline Pr_4MnSb_9. Blue solid, field cooled; blue open square, zero field cooled; red, ferrimagnetic Curie−Weiss fit.

Table 4. Magnetic Data

Magnetic Data	
ferrimagnetic Curie−Weiss fit	
C_A+C_B[a]	8.28(3)
$2\ \mu C_A C_B$[a]	35.01(3)
T_C[a](K)	74.27(8)
χ_0 (emu/mol)[a]	0.06(1)
μ_{eff} (μ_B)[b]	8.13(5)

[a]Obtained from fitting the inverse susceptibility data for H_a = 1000 Oe from 73 to 300 K with the equation $\chi = [(C_A + C_B)T - 2\mu C_A C_B]/(T^2 - T_C^2) + \chi_0$. [b]Calculated from the equation $\mu_{eff} = (7.99(C_A + C_B))$. The theoretical value for 4 Pr^{3+} ions and Mn^{3+} ions is 8.67 μ_B from the equation $\mu_{eff} = (4\ \mu_{Pr^{3+}}{}^2 + \mu_{Mn^{3+}}{}^2)$.

Figure 6 shows the isothermal magnetization and the hysteresis loops of the polycrystalline Pr_4MnSb_9 sample at 2 and 60 K, which demonstrates that this compound is not paramagnetic, and a long-range ferrimagnetic ordering in the title compound may exist. Besides, the field cooled (FC) and zero field cooled (ZFC) data are not consistent below 75 K, which demonstrates that there may be a ferrimagnetic component. (Figure 5) On the basis of this, we conclude that Pr_4MnSb_9 is ferrimagnetic.

Thermal Stability. The TG and DTA results reveal that compound Pr_4MnSb_9 does not decompose irreversibly below 1200 K under the experimental conditions. (Figure 7) The endothermic and exothermic peaks appearing around 873 and 826 K in the DTA curve can be assigned as the thermal behavior related to the melting and solidification. No phase-transition was accordingly observed below 800 K. After the thermal analysis measurement, the sample was quenched in cold water, which is still almost a pure phase of Pr_4MnSb_9 (Supporting Information, Figure S3).

Electrical Conductivity and Seebeck Coefficient Measurements. The polycrystalline powders of Pr_4MnSb_9 were cold-pressed into a pellet about ∼73% of the theoretical density, on which the electrical and thermal transport properties were measured from room temperature to 403 K to ensure no decomposition occurs. The electrical conductivity is about 370 S/cm at room temperature, which increases monotonically with the temperature increase as shown in Figure 8a. The Seebeck coefficient is ∼+5.5 μK/V at room temperature, and increases almost linearly with the temperature increase and reaches ∼+7.7 μK/V at 403 K (Figure 8b). These

dx.doi.org/10.1021/ic400209x | Inorg. Chem. 2013, 52, 7441−7447

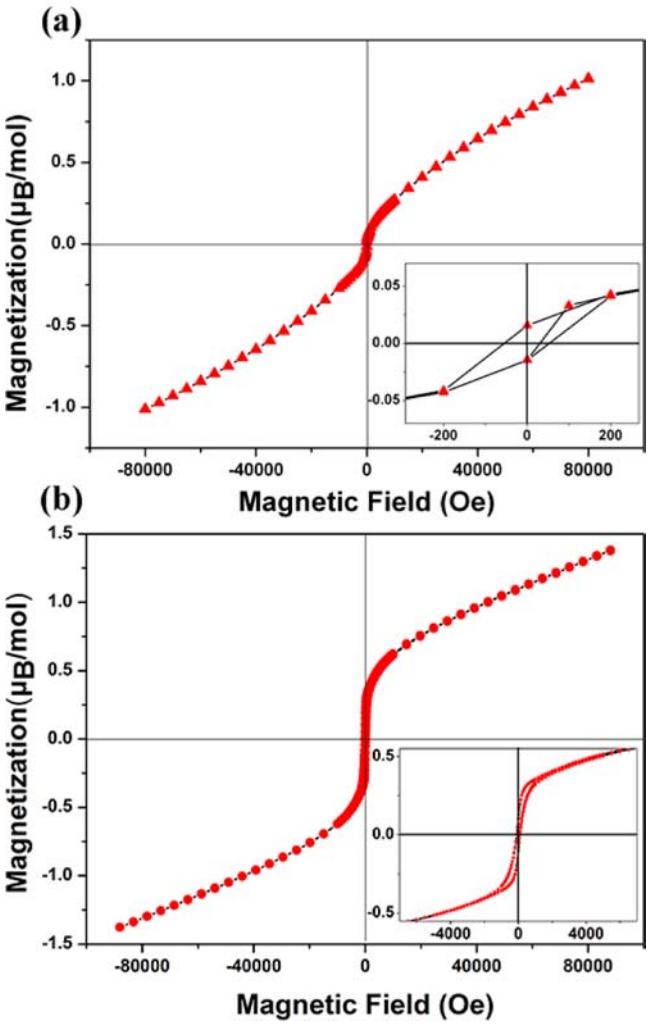

Figure 6. Hysteresis loops of polycrystalline Pr_4MnSb_9 at (a) 2 K, and (b) 60 K.

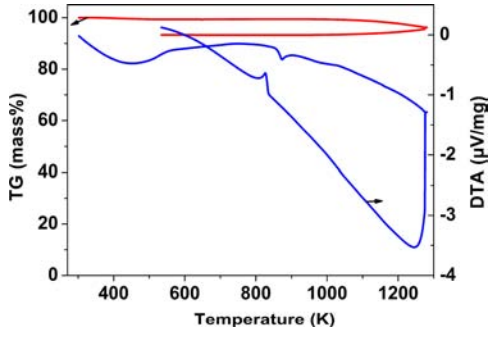

Figure 7. TG and DTA data measured on polycrystalline Pr_4MnSb_9 under the protection of N_2 gas flow from 300 to 1273 K.

values are comparable with the −3.8 μK/V of $BaCu_{7.31(3)}Sb_5$ at room temperature.[28] After the measurement, the sample is still a pure phase according to the powder XRD pattern (Supporting Information, Figure S4). The positive Seebeck coefficient indicates that Pr_4MnSb_9 is a p-type conductor dominated by holes. Since the density of the pellet is pretty low, precise data should be measured on a denser specimen, such as a hot pressed pellet. Nevertheless, the metallic feature is revealed.

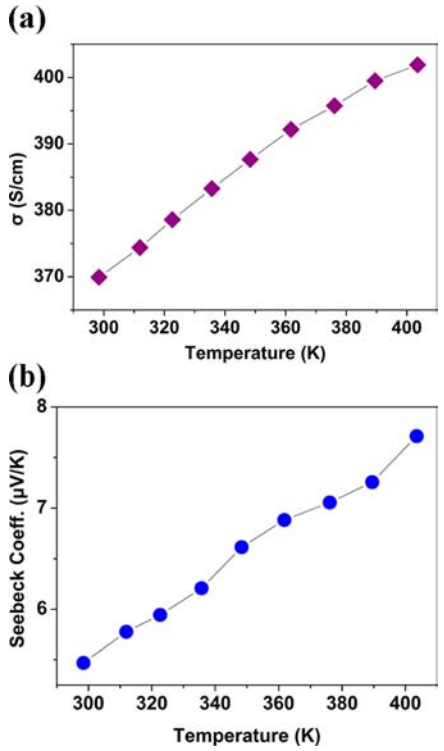

Figure 8. (a) Electrical conductivity and (b) Seebeck coefficient measured on a cold-pressed polycrystalline Pr_4MnSb_9 pellet.

Electronic Structures. The spin-polarized density of states (DOS) and the crystal orbital Hamilton populations (COHP)[29] are studied and displayed in Figures 9 and 10,

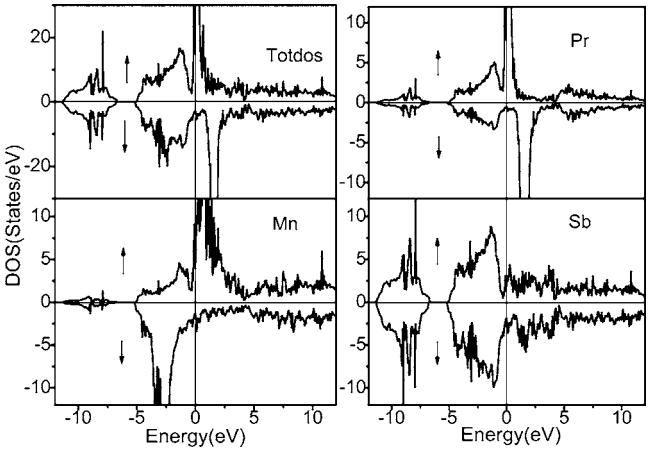

Figure 9. Spin-polarized total and partial density of states (DOS) of Pr_4MnSb_9. The Fermi level is at 0 eV. Upward arrow, spin-up bands; downward arrow, spin-down bands.

respectively. The nonvanishing DOS at the Fermi level indicates that Pr_4MnSb_9 is a metal. In the region from −5 eV to E_F, the significant mixture of Mn-3d and Sb-5p states implies a strong covalent Mn−Sb bonding interaction. Most of the Pr-4f states locate above E_F as expected for an electropositive element. The COHP plots better visualize the hybridization between atom pairs that allow bonding, nonbonding, and antibonding states to be visualized on the energy axis. As generally accepted, a negative COHP indicates bonding interaction and a positive one indicates antibonding interaction.

dx.doi.org/10.1021/ic400209x | Inorg. Chem. 2013, 52, 7441−7447

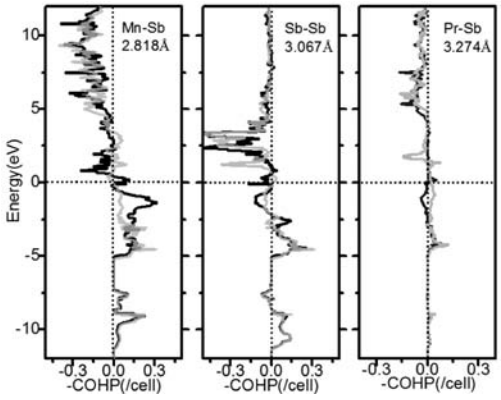

Figure 10. Crystal orbital hamilton population (COHP) of some selected interactions in Pr_4MnSb_9. All curves have been shifted so that the Fermi level energy lies at zero.

The bonding strength between the same pair of atoms can be evaluated by the integrated COHP (ICOHP) values. For a certain pair of atoms, the more negative the ICOHP, the stronger the bond interactions. As shown in Figure 10, solid curves correspond to the bonding interactions between the spin-up states, and dotted curves represent those between the spin-down states. The COHP curves indicate that the Mn−Sb (2.818 Å) bonding states are filled, and no antibonding state is occupied below E_F. The Mn−Sb bonds have an averaged ICHOP of −0.67 eV/(cell·spin). The interaction between Mn and the three-atom-wide tag, B, that is, Mn−Sb7 exhibits an ICOHP of −0.87 eV/(cell·spin) indicating a strong interaction (Supporting Information, Table S2). The Sb−Sb interactions in the range of 3.05−3.15 Å have ICOHP values from −0.33 to −0.62 eV/(cell·spin), which indicate considerable bonding interactions (Supporting Information, Table S2). The covalent component in the Pr−Sb interaction is confirmed to be weak.

CONCLUSION

A new ferrimagnetic valence precise antimonide Zintl phase, Pr_4MnSb_9, with its own structure type has been discovered by high-temperature solid state reactions. The polyanionic 3D network is constructed by strong Sb−Sb and Mn−Sb covalent bonding interactions. Such a network is confined by two types of five-atom-wide Sb_5^{7-} ribbons (denoted as A, C) that are joined by 6-fold coordinated Mn^{3+} cations, that are also linking the narrower three-atom-wide Sb_3^{5-} ribbons as tags of the network. And Pr^{3+} cations and the single Sb^{3-} anions locate within the tunnels as interstitials. Structure relationships between the related compounds are discussed. Interestingly, Pr_4MnSb_9 exhibits ferrimagnetic property. Its metallic feature is supported by the electrical conductivity and Seebeck coefficient measurements and the band structure analyses.

ASSOCIATED CONTENT

Supporting Information

The cif data, EDX, XPS data, and additional figures and tables. This material is available free of charge via the Internet at http://pubs.acs.org.

AUTHOR INFORMATION

Corresponding Author

*E-mail: chenl@fjirsm.ac.cn. Tel: (011)86-591-83704947.

Notes

The authors declare no competing financial interest.

ACKNOWLEDGMENTS

This research was supported by the National Natural Science Foundation of China under Projects 21225104, 20973175, 21171168, 21233009 and the "Knowledge Innovation Program of the Chinese Academy of Sciences" (Grant KJCX2-YW-H20). We thank Prof. Zhang-Zhen He at FJIRSM for the very helpful discussion on the magnetic property.

REFERENCES

(1) Sologub, O. L.; Salamakha, P. S. In *Handbook on the Physics and Chemistry of Rare Earths*; Gschneidner, K. A., Jr., Bünzli, J. C. G., Pecharsky, V. K., Eds.; Elsevier: Amsterdam, The Netherlands, 2003; Vol. 33. pp 35−146.
(2) Mills, A. M.; Lam, R.; Ferguson, M. J.; Deakin, L.; Mar, A. *Coord. Chem. Rev.* **2002**, *233−234*, 207−222.
(3) (a) Papoian, G. A.; Hoffmann, R. *Angew. Chem., Int. Ed.* **2000**, *39*, 2408−2448. (b) Jeitschko, W.; Altmeyer, R. O.; Schelk, M.; Rodewald, U. C. *Z. Anorg. Allg. Chem.* **2001**, *627*, 1932−1940. (c) Tkachuk, A. V.; Tam, T.; Mar, A. *Chem. Met. Alloys* **2008**, *1*, 76−83.
(4) Papoian, G.; Hoffmann, R. *J. Am. Chem. Soc.* **2001**, *123*, 6600−6608.
(5) Kleinke, H. *Chem. Soc. Rev.* **2000**, *29*, 411−418.
(6) Morozkin, A. V. *J. Alloys Compd.* **2003**, *360*, L1−L2.
(7) Morozkin, A. V.; Nirmala, R.; Malik, S. K. *J. Alloys Compd.* **2005**, *394*, 75−79.
(8) Chan, J. Y.; Wang, M. E.; Rehr, A.; Kauzlarich, S. M.; Webb, D. *Chem. Mater.* **1997**, *9*, 2131−2138.
(9) Chan, J. Y.; Olmstead, M. M.; Kauzlarich, S. M.; Webb, D. *Chem. Mater.* **1998**, *10*, 3583−3588.
(10) Holm, A. P.; Park, S. M.; Condron, C. L.; Olmstead, M. M.; Kim, H.; Klavins, P.; Grandjean, F.; Hermann, R. P.; Long, G. J.; Kanatzidis, M. G..; Kauzlarich, S. M.; Kim, S. J. *Inorg. Chem.* **2003**, *42*, 4660−4667.
(11) Brown, D. E.; Johnson, C. E.; Grandjean, F.; Hermann, R. P.; Kauzlarich, S. M.; Holm, A. P.; Long, G. J. *Inorg. Chem.* **2004**, *43*, 1229−1234.
(12) Rühl, R.; Jeitschko, W. *Mater. Res. Bull.* **1979**, *14*, 513−517.
(13) Morozkin, A. V.; Isnard, O.; Henry, P.; Granovsky, S.; Nirmala, R.; Manfrinetti, P. *J. Alloys Compd.* **2006**, *420*, 34−36.
(14) Cordier, G.; Schäfer, H.; Woll, P. Z. *Naturforsch. B: Anorg. Chem. Org. Chem.* **1985**, *40*, 1097−1099.
(15) Sologub, O.; Hiebl, K.; Rogl, P.; Bodak, O. *J. Alloys Compd.* **1995**, *227*, 40−43.
(16) Malik, S. K.; Chu, Z.; Joshi, A. G.; Yang, J. B.; Yelon, W. B.; Cai, Q.; James, W. J.; Kanaraju, K. *J. Appl. Phys.* **2002**, *91*, 7842−7844.
(17) Sologub, O.; Vybornov, M.; Rogl, P.; Hiebl, K.; Cordier, G.; Woll, P. *J. Solid State Chem.* **1996**, *122*, 266−272.
(18) Godart, C.; Rogl, P.; Alleno, E.; Goncalves, A. P.; Rouleau, O. *Phys. B* **2006**, *378−380*, 845−846.
(19) Xia, S. Q.; Bobev, S. *Chem. Mater.* **2010**, *22*, 840−850.
(20) Liu, Y.; Chen, L.; Li, L. H.; Wu, L. M.; Zelinska, O. Y.; Mar, A. *Inorg. Chem.* **2008**, *47*, 11930−11941.
(21) *CrystalClear*, version 1.3.5; Rigaku Corp.: The Woodlands, TX, 1999.
(22) Sheldrick, G. M.*SHELXTL*, version 5.1; Bruker-AXS: Madison, WI, 1998.
(23) Gelato, L. M.; Parthe, E. *J. Appl. Crystallogr.* **1987**, *20*, 139.
(24) Tank, G.; Jepsen, O.; Burkhardt, A.; Andersen, O. K. *The TB-LMTO-ASA program*, version 4.7; Max-Planck-Institut für Festkörperforschung: Stuttgart, Germany, 1998.
(25) (a) Takei, W. J.; Cox, D. E.; Shirane, G. *Phys. Rev.* **1963**, *129*, 2008−2018. (b) Lotgering, F. K.; Gorter, E. W. *J. Phys. Chem. Solids* **1957**, *3*, 238−249.
(26) Kittel, C. In *Introduction to Solid State Physics*, 7th ed.; John Wiley and Sons: New York, 1996; pp 458−462.

(27) Holm, A. P.; Olmstead, M. M.; Kauzlarich, S. M. *Inorg. Chem.* **2003**, *42*, 1973−1981.
(28) Zheng, W. Z.; Wang, P.; Wu, L. M.; Chen, L. *Inorg. Chem.* **2010**, *49*, 7491−7496.
(29) Dronskowski, R.; Blöchl, P. E. *J. Phys. Chem.* **1993**, *97*, 8617.